ARTICLE

Photoelectrochemical NADH regeneration using Pt-modified *p*-GaAs semiconductor electrodes

Paolo Stufano,[a] Aubrey R. Paris,[a] and Andrew Bocarsly*[a]

Abstract: Cofactor regeneration in enzymatic reductions is crucial for the application of enzymes to both biological and energy-related catalysis. Specifically, regenerating NADH from NAD^+ is of great interest, and using electrochemistry to achieve this end is considered a promising option. Here we report the first example of photoelectrochemical NADH regeneration at the illuminated (λ >600 nm), metal-modified *p*-type semiconductor electrode Pt/*p*-GaAs. Although bare *p*-GaAs electrodes produce only enzymatically inactive NAD_2, NADH was produced at the illuminated Pt-modified *p*-GaAs surface. At low overpotential (–0.75 V vs. Ag/AgCl), Pt/*p*-GaAs exhibited a seven-fold greater Faradaic efficiency for the formation of NADH than Pt alone, with reduced competition from the hydrogen evolution reaction. Improved Faradaic efficiency and low overpotential suggest the possible utility of Pt/*p*-GaAs in energy-related NADH-dependent enzymatic processes.

Introduction

Enzymes are useful and versatile tools for synthetic chemists. Particularly, oxidoreductases have been investigated for potential applications in reduction processes on both the lab and industrial scale,[1] as shown by a number of extensive reviews.[1-3] The advantages of enzymatic catalysts are well-known and include mild reaction conditions and high specificity.[1,2] The main limitation of redox enzymes is the need to regenerate expensive redox cofactors required for reactions to proceed.[4] Reduced nicotinamide adenine dinucleotide, NAD(P)H, is the natural cofactor used in common enzymatic reduction systems. In the course of a reaction, it is oxidized to form $NAD(P)^+$ which must be reduced back to NAD(P)H in order to maintain a sustainable process. The two-electron conversion between NADH and NAD^+ is depicted in Scheme 1.

Alternative approaches to complex enzymatic (i.e., whole-cell) regeneration[5,6] are required, but those currently available create unwanted byproducts or necessitate complicated workup procedures.[4,7] Chemical and photochemical regenerations have depended on sacrificial oxidants, despite the fact that bio-renewable electron donors have been explored.[8] Consequently, electrochemical methods are promising strategies for cofactor regeneration.[7a,9]

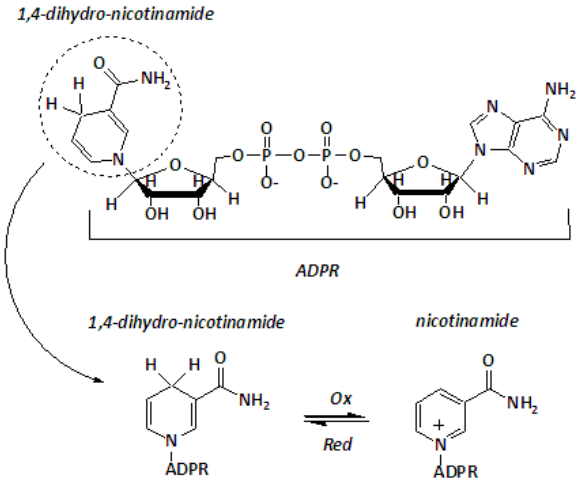

Scheme 1. Structure of NAD^+ (nicotinamide) and two-electron redox conversion between NAD^+ and NADH (1,4-dihydronicotinamide), which occurs in enzymatic processes (ADPR = adenosine diphosphoribose).

Over the past five years, progress has been made in direct electrochemical regeneration of NADH. Specifically, improvements have focused on enhanced selectivity for enzymatically active isomers of NADH, as opposed to the irreversible radical dimerization product NAD_2.[10] Early studies employed organometallic complexes such as $[Cp^*Rh(bpy)H_2O]^{2+}$ as charge mediators, but the deactivating effect of such mediators on enzymes makes the *in situ* regeneration of the cofactor difficult.[7a] Modification of the electrode surface with organic layers gave interesting selectivity results,[11-13] as in the case of cholesterol-modified gold amalgam[12] or L-histidine silver electrodes,[13] but the lack of long-term stability of the modification layer has been problematic.[14] A similar argument holds for surfaces modified by immobilized enzymes or metal complexes.[16,17] Both electroenzymatic[18,19] and enzyme-supported[20] NADH regeneration processes have also been reported, though these studies often sacrifice turnover frequency for selectivity and low applied potential, or vice versa.[20–22] Consequently, several studies began focusing on “all-solid” systems for electrochemical NADH regeneration. For instance, researchers have found success optimizing immobilized carbon nanofibers,[17] various metal electrodes,[23] and either glassy carbon[24,25] or metal electrodes[14,26] patterned with alternative metal nanoparticles.[27–28] In general, these studies have reported an improved ability to adsorb active hydrogen on electrode surfaces, contributing to more effective NADH regeneration as opposed to unwanted dimerization. Nonetheless, high overpotentials are still required by these systems to reduce NAD^+, and limited expansion into fully photochemical NADH

[a] Dr. Andrew Bocarsly, Paolo Stufano, Aubrey Paris
Department of Chemistry
Princeton University
Frick Laboratory, Princeton, New Jersey 08544
E-mail: bocarsly@princeton.edu

Supporting information for this article is given via a link at the end of the document.

regeneration still suffers from low turnover and quantum yield.[19,31] Eliminating the need for high energy inputs and reducing competition with hydrogen evolution is critical if NADH regeneration is to be used in future biomimetic energy applications.

Herein we report the reduction of NAD^+ at the *p*-type single crystal semiconductor electrode *p*-GaAs (111B) and demonstrate the effect of surface modification by electrodeposition of platinum to form a Pt/*p*-GaAs interface. Our results suggest that platinizing the surface of the semiconductor directs the selectivity of the reaction toward the formation of NADH instead of the biologically inactive NAD_2 dimer. To the best of our knowledge, this is the first example of NAD^+ reduction at a semiconductor electrode and the lowest reported overpotential for achieving NADH selectivity above 70%.

Results and Discussion

A survey of NAD^+ reduction chemistry occurring at illuminated p-*type III-V semiconductor electrodes*

The redox target site in NAD^+ is the positively charged nicotinamide ring, a substituted pyridinium moiety. We have previously used a *p*-GaP electrode in the pyridinium-catalyzed, photoelectrochemical reduction of CO_2, a process that involved the initial reduction of pyridinium, (E = –0.58 V vs. SCE, pH 5.3).[32] For this reason, *p*-GaP was first selected for the reduction of NAD^+ to NADH (NAD^+/NADH $E^{\circ\prime}$ = –0.557 V vs. SCE).[33] Although the reduction of NAD^+ is thermodynamically favorable at a *p*-GaP electrode, no NAD^+ reduction products were observed after bulk electrolysis using near UV illumination (λ_{max} = 365 nm - LED) at –1.0 V vs. SCE. Neither NADH nor NAD_2 dimers were formed, although a considerable cathodic current was passed. It was assumed that the reduced nicotinamide ring was converted back to the oxidized form by the UV light used to irradiate the electrode. This was shown to be true for 1,4-NADH, as demonstrated by the ^{1}H NMR spectrum of a standard solution in phosphate buffer after irradiation for ~12 h by the same UV-LED used in the photoelectrochemistry experiment. NAD^+ and minor amounts of ADPR and free nicotinamide were detected, in agreement with findings published by Vitinius *et al*.[34] UV light was employed in the initial photoelectrochemistry study to excite the direct band gap transition in *p*-GaP (2.3 eV).[35] By using a lower energy light (λ_{max} = 465 nm) the indirect band gap transition could be excited. This led to the reduction of NAD^+ to dimeric species, but the conversion was extremely slow. The smaller band gap semiconductors *p*-GaAs and *p*-InP were then tested as photocathodes. ^{1}H NMR analyses revealed that the main product after bulk electrolysis at –1.0 V vs. SCE under red light (λ_{max} = 625 nm) irradiation was 4,4'-NAD_2 at all semiconductor electrode interfaces; no 1,4-NADH was produced.

In an effort to alter the observed reaction trajectory to favor NADH production, a *p*-GaAs surface was modified by electroplating a small amount of ruthenium (at –0.2 V vs. SCE, from $RuCl_3$ aqueous solution, 0.5 M H_2SO_4) onto the semiconductor. This process dramatically changed the selectivity of NAD^+ reduction, making 1,4-NADH the major reaction product, as shown in Figure 1 using ^{1}H NMR analysis of a post-electrolysis reaction mixture. This figure exhibits the characteristic 1,4-NADH ^{1}H NMR signals at 2.55 ppm (pseudo-quartet, 2 H in position 4 of the nicotinamide ring) and 6.75 ppm (singlet, 1 H in position 2). Although the Ru layer facilitated the production of NADH, inactive dimer product was also detected.

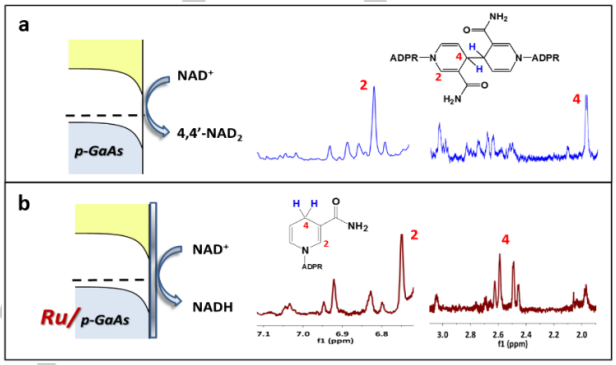

Figure 1. ^{1}H NMR spectra of solutions post-electrolysis performed using (a) *p*-GaAs and (b) Ru-modified *p*-GaAs electrodes. NAD_2 dimer and NADH were generated by *p*-GaAs and Ru-modified *p*-GaAs, respectively. Photoelectrochemical experiments utilized solutions of 0.125 M, pH 7 phosphate buffer and 1 mM NAD^+, an applied potential of –1.0 V vs. SCE, and irradiation with 625-nm red light for 15 h at room temperature.

Platinized p-*type GaAs semiconductor electrodes*

Based on our survey results, metalized *p*-GaAs (E_{BG} = 1.42 eV)[35] was selected for further study as a promising photocathode material. GaAs has been extensively studied in the past for applications in photoelectrochemical cells and electronics.[35–38] A significant challenge associated with *p*-GaAs is photo-induced surface decomposition, a process that is exacerbated in acidic solutions.[38] Thin layers of metal, such as Pt, have been shown to improve the resistance of semiconductor electrodes to photocorrosion.[38,39] Therefore, we elected to electroplate Pt onto the (111) face of a single crystal *p*-GaAs photocathode by reducing the precursor, Na_2PtCl_4 (10 mM), in aqueous solution using red light illumination (see experimental). The deposition of 50 monolayer equivalents (MLE) of Pt onto the electrode, assuming 1.3 x 10^{15} Pt atoms/cm^2, resulted in a material less susceptible to photocorrosion (Figure S1). Plated electrodes exhibited a small dark current (Figure S2), which can be ascribed to the formation of surface states as previously discussed.[39] The positive effect of Pt electroplating on *p*-GaAs photocurrent indicates that the Pt layer not only acts as a protecting agent against photocorrosion, but it also acts as an electrocatalyst for hydrogen evolution, facilitating charge transfer from the semiconductor surface to solution.[40]

Platinization was carried out on both the gallium-rich GaAs (111A) surface and the arsenic-rich GaAs (111B) surface. The high photocurrent density observed at Pt/*p*-GaAs (111B) indicated that the deposited Pt layer is not thick enough to reduce the intensity of the incident radiation at the GaAs surface. Its thickness must therefore be less than 300 Å, as Pt is transparent up to this value.[40] This assumption was confirmed by the inability of energy dispersive spectroscopy (EDS) to detect Pt on *p*-GaAs (111B). Nevertheless, X-ray photoelectron spectroscopy (XPS) signals of Pt ($4f_{5/2}$ 75 eV; $4f_{7/2}$ 72 eV) were clearly observed, confirming, in addition to the electrochemical evidence, the presence of Pt at the *p*-GaAs surface. Interestingly, the same deposition procedure used to formally generate the same MLEs of Pt on a *p*-GaAs (111A) resulted in a thicker layer of Pt. This layer was clearly detectable by EDS analyses and caused a decrease in the limiting photocurrent due to the shielding of the incident light. Pt/*p*-GaAs (111B) was therefore chosen as the electrode for NADH regeneration instead of the (111A) analog, due to its improved light absorption and consequently higher limiting photocurrent.

It has previously been reported that the morphology of the surface Pt layer can be tuned by changing the electrodeposition parameters. Based on the deposition conditions selected, it was expected that Pt would deposit as a discontinuous layer, leaving bare semiconductor sections exposed.[42] However, preliminary experiments showed a relatively homogeneous Pt layer using the deposition conditions noted above. Starting from the same precursor, we decided to employ two different Pt deposition methods. The first method involved potentiostatic deposition at low cathodic potential (i.e., –0.2 V vs. SCE). The second method was a potentiodynamic Pt reduction with 1-s current pulses at a range of applied potentials up to –0.8 V vs. SCE. The formal quantity of Pt loaded was kept constant at 50 MLE by adjusting the total charge passed.

SEM imaging, presented in Figure 2, clearly showed the difference in surface morphologies of the Pt/*p*-GaAs samples obtained by the different deposition techniques. The surface of Pt/*p*-GaAs obtained by potentiostatic deposition at –0.2 V vs. SCE exhibited more complete coverage at the micron and sub-micron scale. On the contrary, the surfaces of Pt/*p*-GaAs derived from pulsed potentiodynamic deposition were even less homogeneous and characterized by small Pt aggregates around 20–25 nm in diameter. This electrode surface morphology closely resembled the Ru-,[26c,d] Pt-, and Ni-GC[27] electrodes utilized by Omanovic and the Ru-GC electrodes employed by Rahman.[30] The authors postulated that islands of materials having low overpotentials for hydrogen evolution could act as H-adsorbed donors for the protonation/reduction of the intermediate radical $NAD^{\bullet}$ and, at the same time, serve as a physical barrier to avoid the dimerization of radicals formed at the surface.[19,26,27] The same argument was invoked for Pt-Au electrodes, although no information about the surface morphology was explicitly reported.[19]

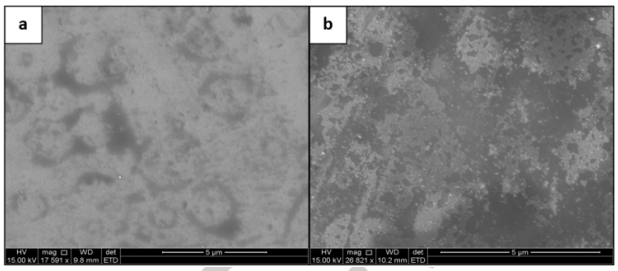

Figure 2. SEM images of Pt-deposited *p*-GaAs synthesized by (a) potentiostatic and (b) pulsed-potentiodynamic methods. Potentiostatic deposition resulted in a more complete Pt layer (visible in light gray), whereas pulsed-potentiodynamic deposition caused the formation of Pt islands on the darker semiconductor surface.

NAD^+ reduction at platinized p*-type GaAs*

Pt/*p*-GaAs was used as a photocathode for NAD^+ reduction in phosphate buffer at pH 7 under 625 nm irradiation and at applied potentials of either –0.95, –0.85, or –0.75 V vs. Ag/AgCl; Pt mesh was employed as the counter electrode. NADH was observed to form at all of these potentials. The conversion of NAD^+ was examined by ^{1}H NMR and normalized with respect to the electrode surface area. As reported in Figure 3a, the conversion of NAD^+ at Pt/*p*-GaAs was approximately 1.2 times larger than that at a Pt foil electrode. No substantial potential dependence was noted for the conversion ratio in the potential range examined. More interestingly, the charge passed at Pt/*p*-GaAs to obtain this higher conversion was less than the charge passed using Pt foil, as seen in Figure 3b. The ratio of charge passed between Pt/*p*-GaAs and Pt foil ranged from 0.6 at more negative potentials to 0.17 at less negative potentials. Thus, there is an increased Faradaic efficiency for NAD^+ reduction at the platinized *p*-GaAs photocathode, which was further enhanced at low overpotentials.

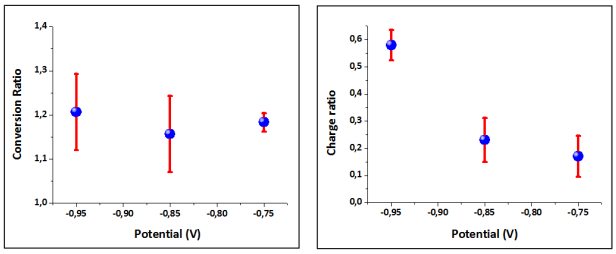

Figure 3. NAD^+ conversion (left) and charge-passed (right) presented as a ratio between red light-illuminated Pt/*p*-GaAs and a Pt foil electrode held at the same potential. Higher conversion efficiencies were achieved at lower overpotentials for Pt/*p*-GaAs. Error bars represent the standard deviation over three experiments.

Pt/*p*-GaAs electrodes prepared by both potentiostatic and potentiodynamic Pt deposition were tested for NAD^+ reduction ability, providing the results given in Figure 4. Thus, the best electrode in terms of Faradaic efficiency was the Pt/*p*-GaAs having a more continuous layer of Pt at the surface, with the heterogeneous Pt film providing approximately the same Faradaic efficiency once high overpotentials were applied. At the least negative regeneration overpotential employed (–0.75 V vs. Ag/AgCl), the potentiostatically deposited Pt/*p*-GaAs exhibited a Faradaic efficiency for NAD^+ reduction that was seven times higher than that of a Pt foil (Figure 4b). This improvement in Faradaic efficiency is presumably due to the fact that at the Pt metal electrode the hydrogen evolution reaction is so efficient that the buffer can no longer maintain neutral pH. In support of this conclusion, it was observed that the final pH measured at the end of NAD^+ reduction at –0.95 V vs. Ag/AgCl was 10.5; the solution pH after the same reaction at Pt/*p*-GaAs was 7.5. Thus, the use of Pt/*p*-GaAs is not only advantageous in terms of its ability to convert optical energy to chemical energy via NAD^+ reduction, but also because it minimizes the variation of solution pH. The latter is a crucial factor for enzyme activity and for NAD^+ stability, which is compromised in basic solutions due to the dissociation of the nicotinamide moiety.[43]

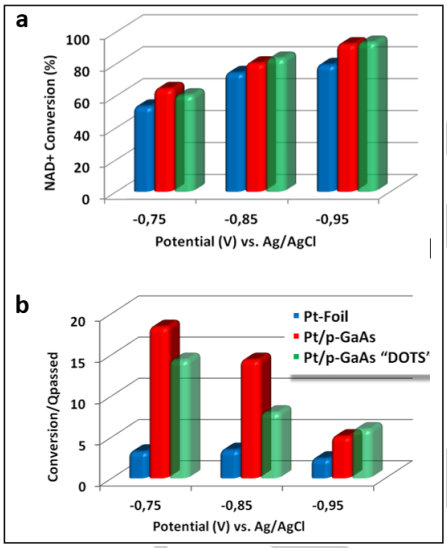

Figure 4. NAD^+ conversion (a) and Faradaic efficiency (b) achieved using Pt/*p*-GaAs (synthesized using either potentiostatic or pulsed potentiodynamic Pt-deposition measures) and Pt foil electrodes. Faradaic efficiency for NADH generation was greatly improved and hydrogen evolution competition reduced using the semiconductor electrodes.

The behaviors of Pt and platinized semiconductor electrodes were compared by linear sweep voltammetry in the absence and presence of NAD^+, as seen in Figure 5a,c. When using Pt foil, no change in the current trace was observed in the presence of NAD^+, while at Pt/*p*-GaAs an increase in cathodic current was measured with increasing NAD^+ concentration up to 20 mM, especially at low overpotentials. This can be understood as the difference between a highly efficient hydrogen evolution reaction occurring at the Pt electrode, versus the Pt/*p*-GaAs electrode on which the hydrogen evolution reaction competes with an efficient NAD^+ reduction. The kinetics of the latter process were also monitored by the absorbance at 340 nm, the characteristic absorbance of reduced nicotinamide species. At Pt/*p*-GaAs it was possible to observe the expected potential dependence on the reduction of NAD^+, while at Pt foil no such dependence was observed. This evidence, portrayed in Figure 5b,d, confirmed that at a Pt foil, NAD^+ reduction is only a side reaction of hydrogen evolution, so that the initial rate of NAD^+ reduction appears independent of the applied reduction potential.

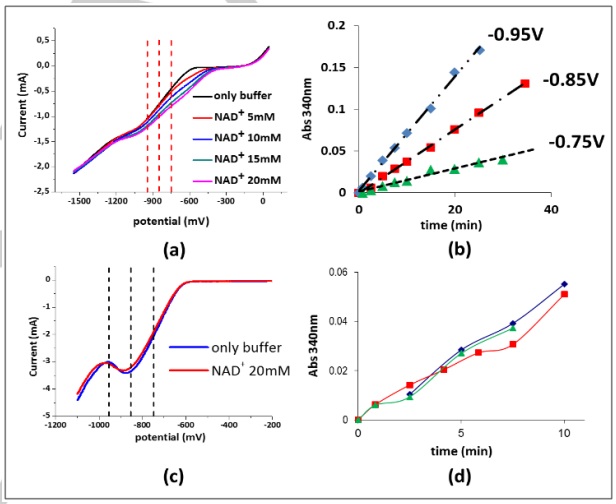

Figure 5. Linear sweep voltammetry at illuminated (a) Pt/*p*-GaAs and (c) Pt foil cathodes in the absence and presence of NAD^+. Absorbance at 340 nm was monitored as an indicator of reaction progress during bulk electrolysis with (b) Pt/*p*-GaAs and (d) Pt foil cathodes. Hydrogen evolution is the dominant reaction using Pt foil cathodes, whereas NADH generation is more competitive when Pt/*p*-GaAs is used.

Prior studies of NADH regeneration at metallic Pt electrodes—as opposed to the Pt/Al_2O_3 system coupled with alcohol dehydrogenase, which exhibited 100% selective generation of 1,4-NADH at low TOF[20]—only partially characterized the products obtained. Yun *et al.*[12,44] reported that enzymatically active NADH was produced with a selectivity of 65–70%. A similar value (63%) was obtained by Damian *et al.*[14] at a Pt/Au electrode. In both of these works, the amount of enzymatically active NADH in the product mixture was determined by enzymatic assay using *D*-lactate dehydrogenase or lipomide dehydrogenase, both of which consume 1,4-NADH selectively. Consequently, the 1,4-NADH content was selectively measured, and the assay provided no information about the coproducts of NADH in the reaction mixture. Instead, it was assumed that the coproducts were mostly

NAD_2 with some 1,6-NADH, according to the work of Jaegfeldt.[45] Possible NAD^+ reduction products are depicted in Scheme 2.

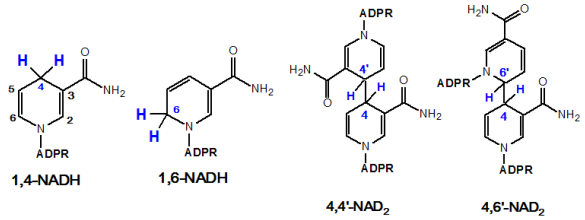

Scheme 2. Potential products achieved during the reduction of NAD^+.

We have analyzed post-bulk electrolysis reaction mixtures at Pt foil and Pt/*p*-GaAs electrodes by ^1H NMR, focusing on the typical signals for the reduced nicotinamide's H2 proton and the proton in the reduced position (i.e., H4 for 1,4-NADH and both 4,4'- and 4,6'-NAD_2; H6 for 1,6-NADH and 4,6'-NAD_2). This analysis and comparison with $NaBH_4$-reduced NAD^+ (Figure S3) indicated that the products of Pt/*p*-GaAs-mediated NAD^+ reduction were 1,4- and 1,6-NADH. Based on ^1H NMR integration referenced to an imidazole internal standard, we calculated a maximum selectivity of 72% ± 1% for the enzymatically active 1,4-NADH. Selectivity is well-retained in the range of potentials examined (i.e., –0.95 to –0.75 V vs. Ag/AgCl), such that a total 1,4-NADH yield of 65% ± 1% was obtained at –0.95 V. These are the highest selectivity yields reported to-date for photoelectrochemical regeneration of NADH. Additionally, our mildest applied potential (–0.75 V vs. Ag/AgCl) is the lowest utilized in the literature to achieve NADH regeneration at >70% selectivity for biologically active 1,4-NADH.

It is worth noting that the product distributions achieved using both Pt foil and Pt/*p*-GaAs electrodes were the same. However, the complete absence of formation of the NAD_2 dimer species at both Pt and Pt/*p*-GaAs interfaces introduces a question about the reaction mechanism for NAD^+ reduction at Pt electrode surfaces. For this reason, we investigated the mechanism of NAD^+ reduction at Pt foil as a model Pt electrode surface.

NAD^+ reduction mechanism at a Pt electrode surface

The mechanism of NAD^+ reduction to NADH has been studied at a variety of metal electrodes,[33,46,47] leading to a commonly accepted reduction mechanism adopted by several of these systems, which is depicted in Scheme 3. Notably, this mechanism involves the formation of a $NAD^\bullet$ intermediate.

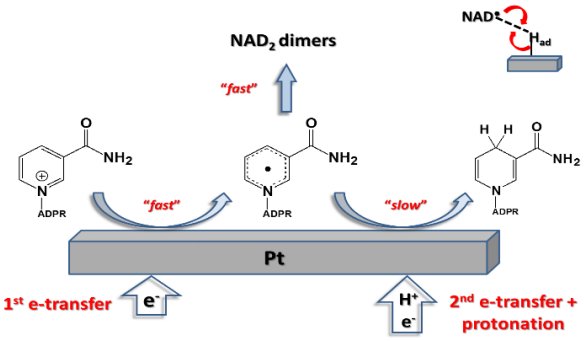

Scheme 3. Common mechanism of the two-electron reduction of NAD^+ to NADH involving the $NAD^\bullet$ intermediate.

In some of these previous works, it was speculated that redox activity of NAD^+ at an electrode interface involves the unfolding of the NAD^+ conformer at the electrode surface, with the adenine moiety then adsorbing onto the surface followed by charge transfer to the nicotinamide ring.[26d,46] Other work suggested that the Pt surface shows negligible adsorption of NAD^+.[47a] Although very negative potentials were required to produce NADH instead of the dimer on Hg electrodes, in the present study no dimeric species were observed at a Pt electrode with an applied potential of only –0.7 V vs. SCE. This raises doubts about the formation of a $NAD^\bullet$ intermediate at the Pt surface since, if it is formed, its dimerization should be much faster ($k > 10^7\ M^{-1}s^{-1}$) than the second one-electron reduction to NADH, especially at such positive electrode potentials. We have therefore investigated the electrochemistry of NAD^+ at a Pt foil electrode. In this study, we find that NAD^+ is efficiently reduced to NADH during a bulk electrolysis at –0.7 V vs. SCE, but no response for NAD^+ is obtained by cyclic voltammetry in the range from –0.9 to 0 V vs. SCE, as shown in Figure 6.

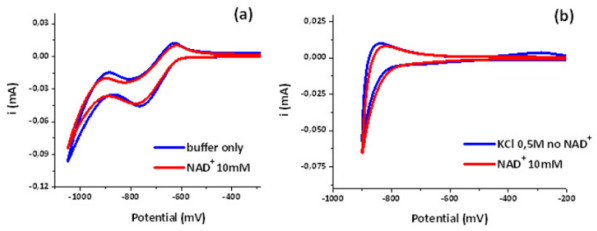

Figure 6. Cyclic voltammograms of 10 mM NAD^+ in (a) 0.125 M phosphate buffer (pH 7) and (b) 0.5 M KCl using a 1 cm^2 Pt foil working electrode.

A reversible wave due to the phosphate buffer itself, in the absence of NAD^+, was detected (Figure 6a). The scan rate dependence of (a) the current function and (b) the anodic to cathodic peak intensity ratio suggest a CE-type mechanism, according to the Nicholson and Shain diagnostic criteria.[48] The half-wave potential of the observed reduction process is consistent with reduction of a weakly acidic phosphate proton to

form a surface-confined hydrogen atom (Equations 1 and 2),[49,50] as shown below:

$H_2PO_4^- + e^- \rightarrow H_{ad} + HPO_4^{2-}$ Equation 1

$H_{ad} + H_2PO_4^- + e^- \rightarrow H_2 + HPO_4^{2-}$ Equation 2

Given that a proton reduction from the buffer occurs at the Pt surface, we suggest that the NAD^+ molecule can then interact with the surface-absorbed H atom formed in this reaction to directly generate NADH. This proposed mechanism is supported by several recent NAD^+ reduction studies,[23,27,28] as well as our own bulk electrolysis and rotating disk experiments.

Bulk electrolysis experiments at –0.8 V vs. Ag/AgCl in 0.5 M KCl without phosphate buffer showed no NAD^+ reduction products. In the presence of 10 mM phosphate buffer, NADH ^{1}H NMR signals were clearly observed, indicating that at such low overpotentials the buffer was necessary for NAD^+ reduction.

The current response of a Pt rotating disc electrode (RDE) is shown in Figure 7. In the absence of NAD^+ the expected linear correlation of $1/i$ with $\omega^{-1/2}$ (where i is the limiting current detected and ω is the angular velocity of the rotating disk electrode) was observed for the reduction of the proton of $H_2PO_4^-$. In the presence of NAD^+, however, a deviation from this trend was observed at low rotation rates, whereas at high rotation speed the curve converged to the one recorded with buffer only. This suggests that at low rotation speeds the reduced proton at the Pt surface has the opportunity to interact with dissolved NAD^+ to form NADH, whereas when the rotation of the electrode generates a rate of mass transport of NAD^+ past the electrode surface which is much faster than the diffusion of NAD^+ to the surface, only proton reduction takes place.

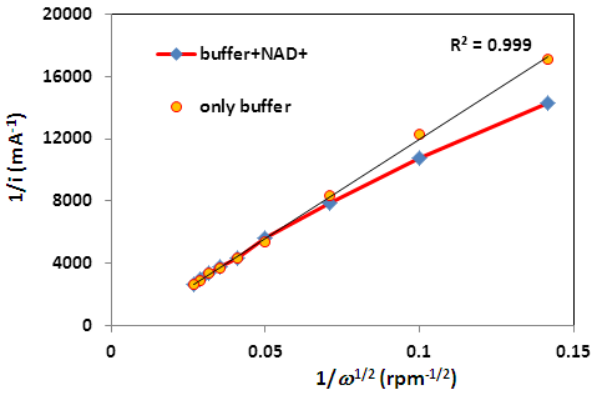

Figure 7. Koutecky-Levich plot (i.e., inverse current vs. inverse square root of angular velocity) obtained using a Pt rotating disk electrode in a solution of phosphate buffer (yellow circles) or buffer plus NAD^+ (blue diamonds).

The reduced proton at the Pt surface could interact with NAD^+ by two possible mechanisms, as depicted in Figure 8. A hydride species could attack the positively charged nicotinamide ring forming NADH directly. This is similar to what happens in the homogeneous reduction of NAD^+ by $NaBH_4$, in which the hydride transfer is the key to avoiding the radical intermediate and, consequently, the NAD_2 formation. Another possible mechanism is the interaction of NAD^+ with an adsorbed H atom on the Pt surface with a coupled electron transfer. The latter mechanism closely resembles the Volmer-Heyrovsky mechanism for the hydrogen evolution reaction.[51] And as previously noted, adsorbed hydrogen playing a considerable role in NADH regeneration has precedent in NAD^+ reduction on surface-modified electrodes.[23,27,28] At this point, the available data does not allow selection of one of these adsorbed hydrogen-assisted mechanisms over the other. However, the absence of a high yield of NAD_2 clearly rules out a simple uncoupled sequence of electron and proton transfers.

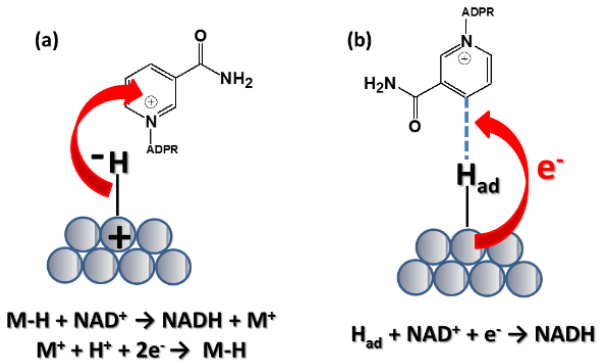

Figure 8. Possible mechanisms of NAD^+ reduction to NADH at a Pt surface by either (a) hydride transfer or (b) adsorbed H/electron transfer.

Conclusions

The photoelectrochemical reduction of NAD^+ at Pt/*p*-GaAs photocathodes has been demonstrated as the first example of semiconductor electrodes for regeneration of enzymatically active NADH. Electrodeposition of a thin Pt layer onto the semiconductor surface facilitated the production of NADH, whereas only NAD_2 dimers were formed at bare *p*-type photocathodes. The Pt/*p*-GaAs electrode exhibited 1.2 times better conversion and 7 times better Faradaic efficiency than a Pt foil electrode at relatively low overpotential. Moreover, it was shown that selectivity for NADH was completely retained at the platinized semiconductor compared with the Pt foil. The products of NAD^+ reduction at Pt surfaces were identified to be the enzymatically active 1,4-NADH (maximum 72% ± 1%) and its isomer 1,6-NADH. The absence of NAD_2 dimers suggests that a mechanism occurs which relies on hydrogen adsorbed to the Pt surface rather than a $NAD^\bullet$ intermediate. Additionally, the absence of organometallic mediators will facilitate the direct coupling of this system with enzymatic reduction processes, such as CO_2 reduction to methanol.

Experimental Section

Chemicals and Materials

β-Nicotinamide dinucleotide (NAD^+) sodium salt from *Saccharomyces cerevisiae*, *β*-nicotinamide dinucleotide reduced (NADH) disodium salt hydrate, K_2HPO_4 (≥ 99.0%), and KH_2PO_4 (≥ 99.0%) were purchased from Sigma-Aldrich and used as received. Phosphate buffer was prepared by mixing appropriate quantities of 1 M K_2HPO_4 and KH_2PO_4 solutions, diluting to the desired buffer concentration, and adjusting the pH to 7 using 0.1 M NaOH solution. All experiments were carried out in oxygen-free solutions by applying a continuous flow of Ar.

Semiconductor wafers were purchased from ITME (Poland). Photocathodes were prepared from a polished and etched piece of *p*-type GaAs [111A] or [111B] Zn-doped to a carrier concentration of 2.16×10^{17}. A layer of 10 nm Ti and 100 nm Au was deposited by e-beam to the etched back of the crystal to form an Ohmic contact. The crystal was then attached to a copper wire with conducting silver epoxy (Epoxy Technology H31). After a thermal cure, the silver epoxy was covered with insulating epoxy cement (Loctite 0151 Hysol) to prevent its exposure to solution during experiments. Prior to deposition of the back contact, platinum deposition, or electrochemical experiments, the semiconductor surface was etched with a freshly prepared solution of concentrated H_2SO_4:H_2O_2 (30%):H_2O (3:1:1 v/v). Platinum was deposited photoelectrochemically (using 625 nm illumination) from a 10 mM aqueous solution of Na_2PtCl_4 hydrate (Sigma-Aldrich) either potentiostatically at –0.2 V vs. SCE or potentiodynamically, calculating the charge necessary to formally deposit 50 MLE assuming 1.35×10^{15} Pt atoms/cm^2.

Typically, working electrodes exhibited a surface area of 0.5 cm^2. Pt electrodes were synthesized by attaching Pt foil and wire (99.99%, Aldrich). SCE or Ag/AgCl electrodes were used as references, and Pt mesh (Sigma-Aldrich) served as a counter electrode.

Instrumentation

A UV-vis Spectrophotometer HP 8453 was used for quantitative analysis of post-bulk electrolysis mixtures by examining the absorption band centered at 340 nm, which appears due to reduction of the nicotinamide ring. Samples were prepared by 1:1 dilution of the product mixtures with 0.125 M phosphate buffer at pH 7.

NMR spectra of solutions after electrolysis were collected on an automated Bruker 500 MHz Spectrometer with an excitation sculpting pulse technique for water suppression. The typical analyte was an aqueous solution containing 10% deuterium oxide (Cambridge Isotope Laboratories, Inc., >99.9%), 0.125 M phosphate buffer, and NAD^+ and its reduction products for a total concentration of 1 mM. MestReNova software was used to process NMR spectra.

An Angstrom Engineering electron beam evaporator was used to deposit back Ohmic contacts on semiconductor wafers.

X-ray photoelectron spectra were collected using a VG Scientific ESCALAB2 spectrometer with monochromated Mg Kα radiation ($h\nu$ = 1253.6 eV). Emitted photoelectrons were detected by a hemispherical analyzer. Operating pressure in the sampling chamber was maintained below 1×10^{-8} Torr. Spectra were collected with a pass energy of 20 eV and data were interpreted using the CasaXPS peak fitting program.

The Quanta 200 FEG ESEM equipped with a Schottky field emission gun (FEG) for optimal spatial resolution and an integrated system for EDS, WDS, and EBSD analysis was used for the surface SEM images of Pt/*p*-GaAs samples. EDX analyses were performed by FEI XL30 FEG-SEM equipped with a PGT-IMIX PTS EDX system, with an optimum image resolution of 2 nm.

Electrochemical Experiments

Cyclic voltammetry, linear sweep voltammetry, rotating disc electrode voltammetry and bulk electrolysis experiments were performed on a CH Instruments 760D electrochemical workstation. Either 0.125 M phosphate buffer or 0.5 M KCl was used as supporting electrolyte. Cyclic voltammograms at Pt foil (0.5 cm^2) or disc (0.1963 cm^2) surfaces were collected at scan rates ranging from 5 to 500 mV/s. Linear sweep voltammetry experiments at illuminated semiconductor electrodes were performed at a scan rate of 20 mV/s.

In a typical bulk electrolysis experiment, a standard, two-compartment H-cell containing a salt bridge between the cathode and anode compartments was used. The reference electrode was placed in the cathode compartment. A 0.5 cm^2-Pt foil or Pt/*p*-GaAs working electrode was used with a Ag/AgCl or SCE reference electrode and Pt mesh counter electrode. The working electrode compartment was filled with 4 mL of 1 mM NAD^+ solution in 0.125 M phosphate buffer and was deoxygenated by bubbling with Ar for several minutes prior to the start of electrolysis. Potentiostatic bulk electrolyses were run at the selected potential for 15 h while irradiating the *p*-GaAs electrode with a Red Luxeon V LED (Future Electronics; λ_{max} = 625 nm). The LED was driven at 700 mA by a Xitanium driver (Advance Transformer Company), and the light was focused with a collimating lens (Future Electronics). Post-bulk electrolysis solutions were analyzed by UV-vis and ^{1}H NMR spectroscopies. Product quantitation by ^{1}H NMR was achieved by integrating characteristic peaks referenced to an imidazole standard.

NAD^+ Reduction by $NaBH_4$

Minor modification of a literature procedure[52] was used to prepare an authentic mixture of 1,2-, 1,4-, and 1,6-NADH isomers. NAD^+ (50 mg) was dissolved in 5 mL of phosphate buffer (0.125 M, pH 7.0) and solid $NaBH_4$ (5 mg) was added, resulting in a color change to yellow-green. The mixture was stirred in air for approximately 10 min, and a sample was directly analyzed by ^{1}H NMR after the addition of 10% v/v D_2O. The target compounds 1,4- and 1,6-NADH, as well as unreacted NAD^+, were identified by the signals of their reduced nicotinamide rings. ^{1}H NMR (H_2O:D_2O 90:10, 500 MHz); 1,4-NADH: δ = 6.75 (H2, s, 1H), 2.56 (H4, m, 2H); 1,6-NADH: δ = 6.93 (H2, s, 1H), 3.65 (H6, m, 2H).

Acknowledgements

The authors acknowledge the United States Department of Energy, Office of Basic Energy Sciences for financially supporting this work under Grant DE-SC0002133. Additionally, ARP acknowledges support by the National Science Foundation Graduate Research Fellowship Program under Grant No. DGE-1148900. Any opinions, findings, and conclusions or recommendations expressed in this material are those of the authors and do not necessarily reflect the views of the National Science Foundation or the US Department of Energy.

Keywords: NADH • cofactor regeneration • photoelectrochemistry • GaAs • semiconductor

[1] F. Hollmann, I.W.C.E. Arends, D. Holtmann, *Green Chem.* **2011**, *13*, 2285.

[2] a) G. W. Huisman, J. Liang, A. Krebber, *Curr. Opin. Chem. Biol.* **2010**, *14*, 122; b) D. Koszelewski, K. Tauber, K. Faber, W. Kroutil, *Trends Biotechnol.* **2010**, *28*, 324; c) K. Faber, S.M. Glueck, B. Seisser, W. Kroutil in *Enzyme Technologies: Metagenomics, Evolution, Biocatalysis and Biosynthesis*, (Eds.: W. K. Yeh, H. C. Yang, J. R. McCarty), John Wiley & Sons, **2010**, pp. 199; d) H. S. Toogood, J. M. Gardiner, N. S. Scrutton, *ChemCatChem* **2010**, *2*, 892.

[3] a) T. Matsuda, R. Yamanaka, K. Nakamura, *Tetrahedron: Asymmetry* **2009**, *20*, 513; b) S. M. A. De Wildeman, T. Sonke, H. E. Schoemaker, O. May, *Acc. Chem. Res.* **2007**, *40*, 1260; c) H. E. Schoemaker, D. Mink, M. G. Wubbolts, *Science* **2003**, *299*, 1694.

[4] a) A. Weckbecker, H. Groger, W. Hummel *Adv. Biochem. Engin./Biotechnol.* **2010**, *120*, 195; b) W. Liu, P. Wang, *Biotech. Adv.* **2007**, *25*, 369; b) R.Wichmann, D.Vasic-Racki, *Adv. Biochem. Engin./Biotechnol.* **2005**, *92*, 225.

[5] a) H. Zhao, W. A. van der Donk, *Curr. Opin. Biotechnol.* **2003**, *14*, 583; b) W. A. van der Donk, H. Zhao, *Curr. Opin. Biotechnol.* **2003**, *14*, 421.

[6] a) W. Kroutil, H. Mang, K. Edegger, K. Faber, *Curr. Opin. Chem. Biol.* **2004**, *8*, 120; b) W. Kroutil, H. Mang, K. Edegger, K. Faber, *Adv. Synth. Catal.* **2004**, *346*,125.

[7] a) F. Hollmann, I.W.C.E. Arends, K. Buehler, *ChemCatChem* **2010**, *2*, 762; b) F. Hollmann, K. Hofstetter, A. Schmid, *Trends Biotechnol.* **2006**, *24*, 163.

[8] A. Dibenedetto, P. Stufano, W. Macyk, T. Baran, C. Fragale, M. Costa, M. Aresta, *ChemSusChem* **2012**, *5*, 373.

[9] R. A. Sheldon, I. W. C. E. Arends, U. Hanefeld, *Green Chemistry and Catalysis*, Wiley-VCH, Weinheim, **2007**.

[10] A. Anne, P. Hapiot, J. Moiroux, J.-M. Saveant. *J. Electroanal. Chem.* **1992**, *331*, 959.

[11] (a) A. A. Karyakin, O. A. Bobrova, E. E. Karyakina, *J. Electroanal. Chem.* **1995**, *399*, 179; (b) K. Warriner, S. Higson, P. Vadgama, *Mat. Sci. Eng.* **1997**, *C5*, 91.

[12] S. H. Baik, C. Kang, I. C. Jeon, S. E. Yun, *Biotech. Techniques*, **1999**, *13*, 1.

[13] Y.-T. Long, H.-Y. Chen, *J. Electroanal. Chem.* **1997**, *440*, 239.

[14] A. Damian, Kh. Maloo, S. Omanovic, *Chem. Biochem. Eng. Q.* **2007**, *21*, 21.

[15] (a) X. Chen, J. M. Fenton, R. J. Fisher, R. A. Peattie, *J. Electrochem. Soc.* **2004**, *151*, E56; (b) S. Kim, S. E-Yun, C. Kang, *J. Electronal. Chem.* **1999**, *465*, 153; (c) S. B. Sobolov, M. D. Leonida, A. Bartoszko-Malik, K. I. Voivodov, F. McKinney, J. Kim, A. J. Fry, *J. Org. Chem.* **1996**, *61*, 2125; (d) A. J. Fry, S. B. Sobolov, M. D. Leonida, K. I. Voivodov, *Tetrahedron Lett.* **1994**, *35*, 5607.

[16] (a) A. Salimi, M. Izadi, R. Hallaj, S. Soltanian, H. Hadadzadeh, *J. Solid State Electrochem.* **2009**, *13*, 485; (b) M. Beley, J.-P. Collin, *J. Mol. Catal.* **1993**, *79*, 133; (c) Y. Shimizu, A. Kitani, S. Ito, *Denki Kagaku*, **1993**, *61*, 872.

[17] I. Ali, M. McArthur, H. Hordy, S. Coulombe, S. Omanovic, *Int. J. Electrochem. Sci.* **2012**, *7*, 7675.

[18] S. Lee, H. Choe, D. H. Cho, S. H. Yoon, K. Won, Y. H. Kim. *J. Electrochem. Soc.* **2016**, *163*, G50.

[19] K. A. Brown, M. B. Wilker, M. Boehm, H. Hamby, G. Dukovic, P. W. King. *ACS Catal.* **2016**, *6*, 2201.

[20] X. Wang, H. H. P. Yiu. *ACS Catal.* **2016**, *6*, 1880.

[21] T. H. Dinh, S. C. Lee, C. Y. Hou, K. Won. *J. Electrochem. Soc.* **2016**, *163*, H440.

[22] S.-H. Kim, G.-Y. Chung, S.-H. Kim, G. Vinothkumar, S.-H. Yoon, K.-D. Jung. *Electrochim. Acta*, **2016**, *210*, 837.

[23] I. Ali, T. Khan, S. Omanovic, *J. Mol. Cat. A.* **2014**, *387*, 86.

[24] I. Ali, S. Omanovic, *Int. J. Electrochem. Sci.* **2013**, *8*, 4283.

[25] I. Ali, S. Omanovic, *J. Solid State Electrochem.* **2014**, *18*, 833.

[26] (a) I. Ali, B. Soomro, S. Omanovic, *Electrochem. Commun.* **2011**, *13*, 562; (b) A. Damian, S. Omanovic, *J. Mol. Catal. A Chem.* **2006**, *253*, 222; (c) A. Azem, F. Man, S. Omanovic, *J. Mol. Catal. A Chem.* **2004**, *219*, 283; (d) F. Man, S. Omanovic, *J. Electroanal. Chem.* **2004**, *568*, 301.

[27] I. Ali, A. Gill, S. Omanovic, *Chem. Eng. J.* **2012**, *188*, 173.

[28] N. Ullah, I. Ali, S. Omanovic, *Mat. Chem. Phys.* **2015**, *149-150*, 413.

[29] A. Sanchez-Iglesias, A. Chuvilin, M. Grzelczak, *Chem. Commun.* **2015**, *51*, 5330.

[30] G. Rahman, S. A. Mian, A. H. A. Shah, O.-S. Joo, *J. Appl. Electrochem.* **2016**, *26*, 459.

[31] K. T. Oppelt, J. Gasiorowski, D. A. M. Egbe, J. P. Kollender, M. Mimmelsbach, A. W. Hassel, N. S. Sariciftci, G. Knor, *J. Am. Chem. Soc.* **2014**, *136*, 12721.

[32] (a) E. E. Barton, D. M. Rampulla, A. B. Bocarsly, *J. Am. Chem. Soc.* **2008**, *130*, 6342; (b) E. Barton Cole, P. S. Lakkaraju, D. M. Rampulla, A. J. Morris, E. Abelev, A. B. Bocarsly, *J. Am. Chem. Soc.* **2010**, *132*, 11539; (c) A. J. Morris, R. T. McGibbon, A. B. Bocarsly, *ChemSusChem* **2011**, *4*, 191.

[33] L. Gorton in *Encyclopedia of Electrochemistry, Vol. 9* (Eds.: A.J. Bard, M. Stratmann), Wiley-VCH, **2002**, pp. 124.

[34] U. Vitinius, K. Schaffner, M. Demuth, M. Heibel, H. Selbach, *Chem. Biodivers.* **2004**, *1*, 1487.

[35] K. Rajeshwar in *Encyclopedia of Electrochemisrty*, *Vol. 6*, (Eds.: A. J. Bard, M. Stratmann), Wiley-VCH, **2002**, pp. 1.

[36] F.-R. F. Fan, A. J. Bard, *J. Am. Chem. Soc.* **1980**, *102*, 3677.

[37] *Electrochemistry of Semiconductors and Electronics*, (Eds.: J. McHardy, F. Ludwig), Noyes Publications, **1992**.

[38] (a) K. W. Frese in *Semiconductor Electrodes,* (Ed.: H. O. Finklea), Elsevier, New York, **1988,** pp. 373; (b) K. W. Frese, M. J. Madou, S. R. Morrison, *J. Electrochem. Soc.* **1981,** *128*, 1939.

[39] (a) P. Allongue, E. Souteyrand, L. Allemand, *J. Electrochem. Soc.* **1989**, *136*, 1027; (b) P. Allongue, E. Souteyrand, *Electrochim. Acta*, **1989**, *34*, 1717.

[40] M. Szklarczyk, J. O'M Bockris, *J. Phys. Chem.* **1984,** *88*, 1808.

[41] J. D. Porter, A. Heller, D. E. Aspnes, *Nature* **1985,** *313*, 664.

[42] A. Heller, *Pure Appl. Chem.* **1986,** *58*, 1189.

[43] B. M. Anderson, C. D. Anderson, *J. Biol. Chem.* **1963**, *253*, 1475.

[44] S.-E. Yun, M. Taya, S. Tone, *Biotech. Lett.* **1994**, *16*, 1053.

[45] H. Jaegfeldt, *J. Electroanal. Chem.* **1980**, *110*, 295.

[46] A. Damian, S. Omanovic, *Langmuir*, **2007**, *23*, 3162.

[47] (a) P. J. Elving, W. T. Bresnahan, J. Moiroux, Z. Samec, *Biolectrochem. Bioenerg.* **1982**, *9*, 365; (b) C. O. Schmakel, K. S. V. Santhanam, P. J. Elving, *J. Am. Chem. Soc.* **1975**, *97*, 5083.

[48] R. S. Nicholson, I. Shain, *Anal. Chem.* **1964**, *36*, 706.

[49] K. Takehara, Y. Ide, T. Nakazato, N. Yoza, *J. Electroanal. Chem.* **1990**, *293*, 285.

[50] Y. Yan, E. L. Zeitler, J. Gu, Y. Hu, A. B. Bocarsly, *J. Am. Chem. Soc.* **2013,** *135*, 14020.

[51] Y. Cai, A. B. Anderson, *J. Phys. Chem. B* **2004,** *108*, 9829.

[52] (a) M. M. Khader, M. M. Saleh, *Thin Solid Films* **1999**, *165*, 349; (b) M. M. Khader, M. M. Hannout, M. S. El-Dessouki, *Int. J. Hydrogen Energy* **1996**, *21*, 547.

Entry for the Table of Contents (Please choose one layout)

Layout 1:

ARTICLE

Electrochemical regeneration of NADH from NAD^+ is a tool for the study of both biochemical and alternate energy processes. Here we report photoelectrochemical NADH generation at an illuminated metal-modified, *p*-type semiconductor electrode, Pt/*p*-GaAs. Although bare *p*-GaAs electrodes produce only enzymatically inactive NAD_2, NADH was efficiently produced at the Pt/*p*-GaAs interface. This system produces one of the highest Faradaic efficiencies for NADH at a solid electrode interface in the absence of a soluble mediator.

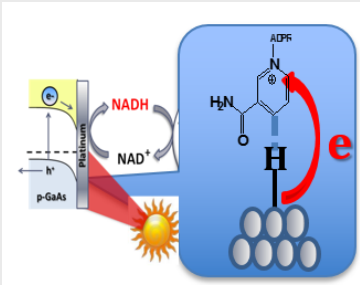

*Paolo Stufano, Aubrey R. Paris, Andrew Bocarsly**

Page No. – Page No.

Photoelectrochemical NADH regeneration using Pt-modified *p*-GaAs semiconductor electrodes

Layout 2:

ARTICLE

((Insert TOC Graphic here))

*Author(s), Corresponding Author(s)**

Page No. – Page No.

Title

Text for Table of Contents